Sixth International Symposium on Marine Propulsors
smp'19, Rome, Italy, May 2019

Hydrodynamic Performance Prediction Method for the Ducted Contra-Rotating Propeller

Hao-peng CAI[1], Cheng-peng HAO[1]，He ZHANG[2]

[1]Key Laboratory of Information Technology for Autonomous Underwater Vehicles, Chinese Academy of Science, Beijing, China
[2]China Ship Research and Development Academy, Beijing, China

ABSTRACT

The ducted contra-rotating propeller (DCRP) is a kind of integrated propulsor unit in which a contra-rotating propeller (CRP) is rotating inside a duct.

A general numerical method of predicting hydrodynamic performance of DCRPs is proposed in this paper. This method is based on the solution of unsteady RANS equations with the SST k-ω turbulence model, using the sliding mesh model to simulate the unsteady interactions between the two blade rows of the CRP, and between the CRP and the surrounding duct. A structured mesh is applied in order to simulate and analyze the flow around the DCRP. Boundary layer meshes are adopted on the CRP's blade surface and duct surface to improve the hydrodynamic performance prediction accuracy.

Numerical predictions are carried out for a DCRP, and results are compared with experimental data. Validation results indicate that the prediction method developed in this article can yield accurate results in both thrust and torque of the DCRP.

Keywords

ducted contra-rotating propellers(DCRP); hydrodynamic performance; numerical prediction; RANS method.

1 Introduction

The ducted contra-rotating propeller (DCRP) is a kind of integrated propulsor unit in which a contra-rotating propeller (CRP) is rotating inside a duct. DCRP is an effective combination of ducted propeller and CRP with the advantage of higher efficiency, larger thrust, better cavitation performance and lower noise level. There is a set of CRP (two rotors) working inside a decelerating duct for the DCRP, and two rotors for DCRP are lighter loaded than only one rotor for the pumpjet propulsor. Therefore, DCRP may has lower critical cavitation number and better noise characteristic than the pumpjet propulsor. Replacing CRPs or pumpjet propulsors, DCRPs have been used in revolution-body-shape underwater vehicles, such as AUVs and torpedoes.

The hydrodynamic performance of DCRPs is an important characteristic in DCRPs' design, for it is strongly correlated to the propulsive efficiency, cavitation inception, and noise and vibration performance of DCRPs. Since the two blade rows of the CRP unit interact with each other and the CRP unit also interacts with the surrounding duct, generating a complicated flow field around the DCRP, it is difficult for the steady and unsteady hydrodynamic performance prediction.

Numerous numerical and experimental researches of marine propulsors such as CRP, the ducted propeller, and the pumpjet propulsor were carried out.

Tsakonas et al (1983) and Yang et al (1991, 1992) applied unsteady lifting surface theory, and Liu (2009) applied the panel method, to predict the steady and unsteady hydrodynamic performance of CRPs. Gu, Su and Kinnas et al (2003, 2017) coupled a potential flow method (vortex-lattice method or boundary element method) and a RANS solver (axisymmetric or non-axisymmetric 3D) to predict the CRPs' and ducted propellers' hydrodynamic performance. Zhang et al (2010, 2011) and Wang (2013) applied RANS method for the steady and unsteady hydrodynamic performance of CRPs considering the effect of variations of CRPs' parameters and calculation settings. Sasaki et al (2009) and Grassi et al (2013) focused on the design and model test method of CRPs.

Hughes and Kinnas (1991) carried out hydrodynamic model tests on a ducted propeller with pre-swirl stator blade, and combined a potential based panel method on the duct and hub with a lifting-surface method on the propeller and stators, to analyze the ducted propeller (single and two-component) flows. J-Baltazar et al (2011) discussed several modelling aspects for the performance predictions of a ducted propulsor with a low-order panel method. Henri et al (2011) utilized a commercial RANSE

* Supported by IACAS Young Elite Researcher Project (QNYC201808)

. Corresponding author. *E-mail address:* caihaopeng@mail.ioa.ac.cn (Hao-peng CAI)

code to predict the ducted propeller open water performance at model scale and full scale, and validated the code by comparison with test results. R-Bontempo et al (2016) employed the axial momentum theory and the nonlinear semi-analytical actuator disk model to analyze the flow around a marine propeller ducted with a decelerating nozzle.

Ivanell (2001) described a CFD model for hydrodynamic performance prediction of the pumpjet propulsor on a torpedo using FLUENT, and verified its precision by comparison with wind tunnel test results. Rao (2012) predicted and analyzed hydrodynamic performance of pumpjet propulsor with pre-swirl stators by mixing plane and sliding mesh method. Suryanarayana et al. (2010a, b) made a CFD analysis of the open water and self-propulsion performance of the pumpjet propulsor on an axisymmetric underwater body, and presented several suggestions for numerical and model test study of the pumpjet propulsor. Lin et al (2016) discussed the pressure distributions around rotor and stator blades of the pumpjet propulsor through a validated CFD method. Motallebi-Nejad M et al. (2017) analyzed the flows around the ducted propeller and pumpjet propulsion system based a numerical CFD method using periodic computational domain.

Those researches played an important role for further researches of numerical analysis of the DCRP. However, present literature review illustrates that the study on numerical simulation or prediction for hydrodynamic performance of the DCRP is far and few between.

In this study, a general numerical method of predicting hydrodynamic performance of DCRPs is proposed. This method is based on the solution of unsteady RANS equations with the SST k-ω turbulence model, using the sliding mesh model to simulate the unsteady interactions between the two blade rows of the CRP, and between the CRP and the surrounding duct. A structured mesh generation strategy is applied to the tip region of CRP in order to simulate and analyze the tip-clearance flow of the DCRP. Boundary layer meshes are adopted on the CRP's blade surface and duct surface to improve the hydrodynamic performance prediction accuracy.

Numerical predictions are carried out for a DCRP utilized for a high-speed underwater vehicle, and results are compared with experimental data. The numerical prediction method and mesh independence inspection is verified. Validation results indicate that the prediction method developed in this article can yield accurate time-averages results in both thrust and torque of the DCRP.

2 Numerical Modeling Approach

2.1 Governing Equations

With DCRPs operation in the uniform flow assumed incompressible and viscous, the governing equations for the turbulent flow field around DCRPs are the instantaneous conservation of mass (continuity equation) and momentum (Reynolds averaged Navier-Stokes equation, RANS). These equations can be expressed as follows:

$$\frac{\partial \rho}{\partial t}+\frac{\partial}{\partial x_i}(\rho u_i)=0 \tag{1}$$

$$\frac{\partial}{\partial t}(\rho u_i)+\frac{\partial}{\partial x_j}(\rho u_i u_j)=-\frac{\partial p}{\partial x_i}+\frac{\partial \tau_{ij}}{\partial x_j}+\frac{\partial}{\partial x_j}\left(-\rho\overline{u_i' u_j'}\right) \tag{2}$$

Where all the variables are time-averaged, and u_i, ρ, p, τ_{ij}, $-\rho\overline{u_i' u_j'}$ are velocity, fluid density, static pressure, shearing stress, Reynolds stress, respectively.

An additional equation is needed to solve the unknown Reynolds stress which ensures the set of governing equations are in closed form. Combining the fluctuating and time average, turbulence model is developed to express or solve the Reynolds stress. SST k-ω model is selected in this paper. SST k-ω turbulence model was developed by (Menter, 1994) to effectively blend the robust and accurate formulation of the standard k-ω model in the near-wall region with the free-stream independence of the standard k-ε model in the far field. As for SST k-ω turbulence model, the computational solver automatically choose different turbulence models based on Reynolds number, specifically, invoking the k-ω turbulence model in the low Reynolds number regions while the k-ε turbulence model in the high Reynolds number regions. Therefore, the SST k-ω turbulence model has its own advantages in solving boundary problems of different Reynolds numbers.

2.2 Mesh Generation and Boundary Condition

As illustrated in Fig.1, The global computational domain is a concentric cylinder which coincides with the DCRP rotating axis. The diameter of the domain is $6D_F$, where D_F is the forward propeller diameter. The inlet is $4D_F$ in length before the forward propeller disk and the outlet is set up at $8D_F$ behind the aft propeller disk. This domain is divided into three cylindrical regions: two independent rotational domains for the CRP, and outer stationary domain including the duct. Those domains can be divided into several sub-domains (or blocks) in order to apply the most appropriate mesh type to ensure better quality and less quantity of discretized cells. Both of outer and inner blocks are made of structured hexahedral cells.

The near-wall boundary layer meshes of the CRP and the duct are 6 layers prismatic cells with the growth ratio of 1.15, while the first layer cell height is carefully set to ensure Yplus valuing in the range of 30 to 90 for propeller blades and duct surfaces. Moreover, the mesh in the region between forward and aft propellers is refined to capture the trailing vortex of the forward propeller more precisely.

Due to the axisymmetric distribution of propeller blades, two rotational domains are further divided into Z portions of identical geometry, where Z is the blade number of the forward/aft propeller. By this further division, the cell distributions in all of the Z portions from the same sub-domain, are identical to each other, thus minimizing the possible calculation error of cell discretization.

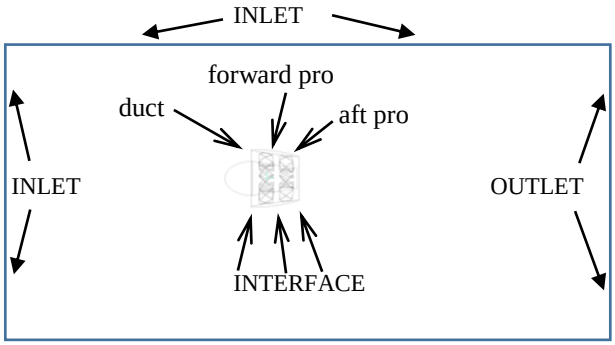

Fig.1-The computational domain and its sub-domains

As shown in Fig.1, the 'inlet' boundaries are defined as velocity inlets, while the 'outlet' boundary as pressure outlet. In the rotating coordinate systems, no-slip wall boundary condition is applied on the surfaces of the CRP and the duct. The flow simulations are carried out using software FLUENT for the RANS equations. Simulation control options are listed in Tab.1. To balance the unsteady simulation time and accuracy, the approximated solution is first reached through the moving reference frame (MRF) technique, then the simulation goes on with the sliding mesh model to get the final simulation solution.

Tab.1-FLUENT Control options setting

CONTROL OPTIONS		SETTING
Solver		Pressure Based
Turbulence model		SST k-ω model
Pressure-velocity coupling		PISO
Unsteady formulation		2nd-order implicit
Turbulent intensity & viscosity ratio (inlet)		0.1% & 1.0
Turbulent intensity & viscosity ratio (outlet)		0.1% & 1.0
Discretization	Gradient	Green-Gauss Cell Based
	Pressure	Presto!
	Momentum	Second Order Upwind
	Turbulent Kinetic Energy	Second Order Upwind
	Specific Dissipation Rate	Second Order Upwind
Under-relaxation factors	Pressure	0.15
	Density	1.0
	Body Force	1.0
	Momentum	0.5
	Turbulent Kinetic Energy	0.5

3. Results and Discussions

A DCRP is selected as the computational geometry of numerical prediction in this study. The DCRP, which was utilized for a high-speed underwater vehicle, consists of an 11-bladed forward propeller and a 9 bladed aft propeller inside a decelerating duct, as shown in Fig.2. The main geometrical features of the DCRP are listed in Tab.2.

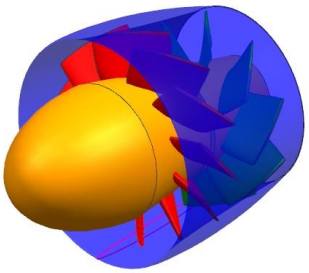

Fig.2-DCRP computational geometry

In the following sections, to be consistent with the hydrodynamic model tests conditions, the rotational speeds of 2500rpm is set in the numerical simulation, and the inlet velocity is varied according to the advance speed coefficient *J*. The thrust coefficients of the forward, aft propeller and the duct are defined as $KT_f = T_f / \rho n^2 D^4$, $KT_a = T_a / \rho n^2 D^4$ and $KT_d = T_d / \rho n^2 D^4$. The torque coefficients of the forward and aft propeller are defined as $KQ_f = |Q_f| / \rho n^2 D^5$ and $KQ_a = |Q_a| / \rho n^2 D^5$, where T_f, T_a and T_d represent the thrust of the forward, aft propeller and the duct, respectively. Q_f and Q_a denote the torque of the forward and aft propeller, respectively. And ρ, n, and D are fluid density, CRP rotational speed, and the forward propeller diameter, respectively. The thrust coefficient and torque coefficient of the DCRP are defined as $KT = KT_f + KT_a + KT_d$ and $KQ = KQ_f + KQ_a$, respectively. The DCRP efficiency $\eta = (J \times KT)/(2\pi \times KQ)$ is defined.

3.1 Mesh Convergence Study

For the mesh convergence study, three structured meshes (coarse, medium, and fine) are generated. To research the influence of the mesh type, an additional unstructured mesh (named fine-unstructured) is also generated. For this unstructured mesh, tetrahedral meshes surrounding the forward and aft propeller replace the hexahedral meshes in CRP domains. Details of the meshes are summarized in Tab.3.

A numerical simulation is performed at the DCRP design point *J*=2.49 using the method mentioned in section2. The convergence histories of the thrust coefficient *KT* and torque coefficient *KQ* for all meshes are shown in Fig.3 and Fig.4, respectively. The time step, t_i/t_{max}, is normalized by the final time step of each specific simulation. It can be shown in these figures that the thrust and torque converge gradually with the simulation carried out. And as the structured mesh is refined both *KT* and *KQ* tend to converge to smaller values, but the value is biggest for both *KT* and *KQ* of the unstructured mesh. Tab.4 shows the numerical simulation results of the DCRP hydrodynamic performance at *J*=2.49. As shown in Tab.4, the simulation results of the medium and fine mesh are close to model test results. The differences of

Tab.2-Geometrical features of Ducted CRPs case

Ducted CRPs——Propeller	forward	aft		Ducted CRPs——Duct	duct
Diameter (mm)	274.5	248.3		Length(mm)	240.0
NO. of blades	11	9		MAX Diameter (mm)	302.2
Pitch ratio (P/D_F) at 0.7R	2.391	2.483		MIN Diameter (mm)	234.6
Hub ratio (dh/D_F)	0.575	0.506		MIN Gap bet. CRPs & Duct (mm)	1.5
Direction of rotation	Right	Left		Axial spacing from Pro-F to L.E.of Duct (A/L_D)	0.316
Axial spacing (a/D_F)	0.363				
Sections	naca66mod+a=0.8			Type	decelerating

coefficients are less than 1% between the medium and fine mesh. For saving computation time, the medium mesh has been selected for numerical prediction and analysis.

Tab.3-Details of mesh cells distribution

Domain	Coarse	Medium	Fine	%	Fine-unstr	%
Forward Pro	2.43M	4.61M	6.1M	35.1	7.21M	36.8
Aft Pro	2.25M	4.22M	5.52M	31.8	6.63M	33.8
Duct	1.13M	2.03M	2.64M	15.2	2.64M	13.5
Near wake field	0.96M	1.74M	2.25M	13.0	2.25M	11.5
Outer	0.35M	0.66M	0.86M	5.0	0.86M	4.4
Total	7.12M	13.26 M	17.37 M	100. 0	19.59 M	100. 0

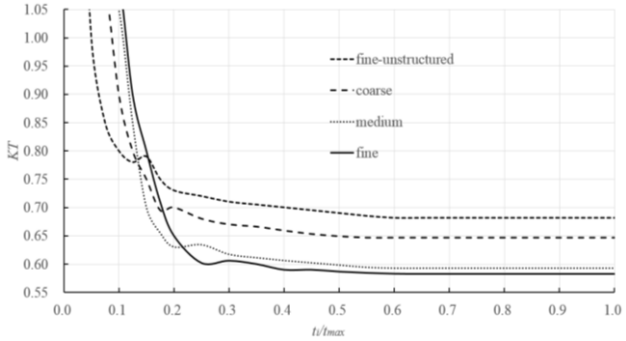

Fig.3-Convergence history of the thrust coefficient

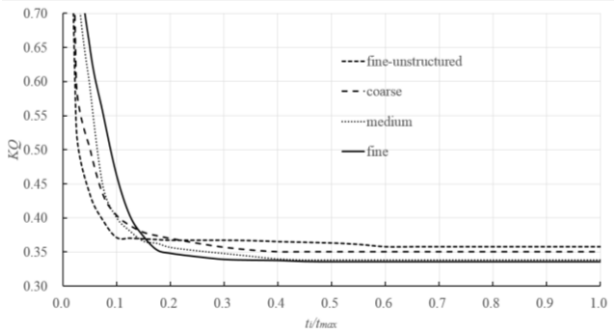

Fig.4-Convergence history of the torque coefficient

Tab.4-Numerical simulation results

MESH	KT_f	KT_a	KT_d	KQ_f	KQ_a
fine-unstructured	0.5057	0.4961	-0.3203	0.1810	0.1769
coarse	0.4940	0.4811	-0.3286	0.1777	0.1726
medium	0.4725	0.4643	-0.3443	0.1712	0.1669
fine	0.4698	0.4603	-0.3475	0.1703	0.1655
model test	0.4622	0.4540	-0.3568	0.1638	0.1608

From Tab.4, we can also see, for the unstructured meshes, the gap between simulation and model test results is relatively larger than that of structured meshes, though the mesh quantity is largest. The reason may be concluded from Fig.5- Fig.6. Take the aft propeller as an example. Fig.5 shows particulars of the structured and unstructured meshes around the propeller tip. Fig.6 draws streamlines in the propeller tip region. More vortex structures can be found for the structured meshes computation, while few vortex structure for the unstructured case. This difference may lead to the prediction error for the unstructured meshes simulation. Maybe the unstructured mesh size in this study is too coarse to simulate and analyze the tip-clearance of the DCRP.

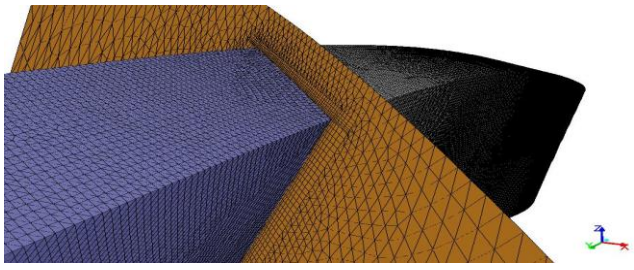

(a) Unstructured mesh surrounding the aft propeller tip

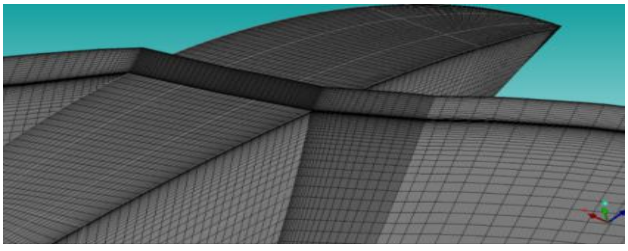

(b) Structured mesh surrounding the aft propeller tip

Fig.5-Structured/unstructured meshes around the propeller tip

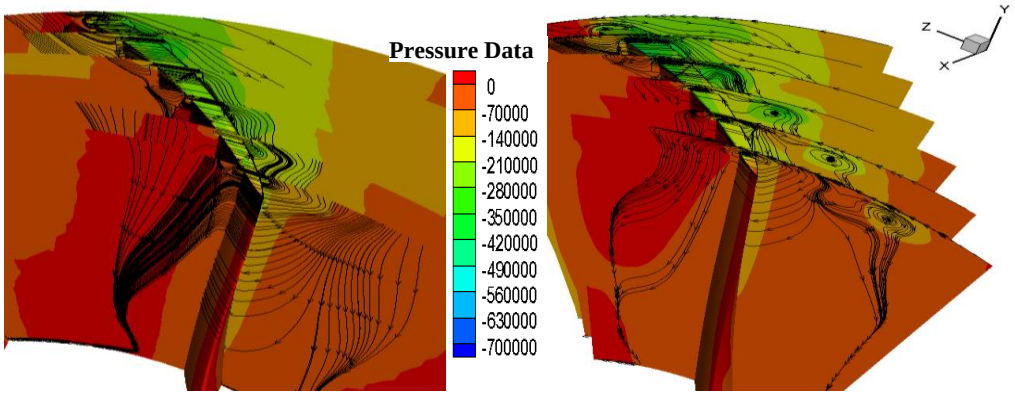

(a) Unstructured mesh case (b) Structured mesh case

Fig.6-Streamlines in the aft propeller tip region

3.2 Time-step Size Study

The basic time-step size is determined by $\triangle t$=1.0/(6×N), (corresponding to a rotation of one degree for the DCRP blade), where N is the rate of revolution per minute. Numerical simulations are carried out with different time-step sizes ($0.5\Delta t$, Δt, $1.5\Delta t$, $2\Delta t$, $3\Delta t$) for different meshes (coarse, medium, fine, fine-unstructured), with 12 internal iterations to accomplish convergence for any given time-step size. Details of the simulation conditions are summarized in Tab.5.

Tab.5-Details of simulation conditions

Time-step size	MESH			
	Coarse	Medium	Fine	Fine-unstr
3×Δt		√	√	
2×Δt		√	√	
1.5×Δt	√	√	√	√
Δt	√	√	√	√
0.5×Δt	√	√		√

Tab.6 shows the numerical simulation results with different time-step sizes. It can be concluded from Tab.6 that for all meshes the time-step size of 1.5×Δt is an appropriate selection for both the simulation accuracy and computation time.

As for DCRPs or CRPs, the frequencies of thrust and torque fluctuation are determined by $f = f_n \times (m_F Z_F + m_A Z_A)$ and subject to $m_F Z_F = m_A Z_A$, where f_n is the shaft frequency, Z_F and Z_A are the blade numbers of the forward and aft propellers respectively, m_F and m_A are positive integers. As for this DCRP case, with 11 blades forward and 9 blades aft, according to the formula $f = f_n \times (m_F Z_F + m_A Z_A)$, the lowest frequency of thrust and torque fluctuation is $f_{\min} = 198 f_n$, which is quite higher than the conventional propeller. Therefore, there are 198 periods of thrust (or torque) fluctuation in a revolution. This means that when the DCRP rotates by 360/198=1.82 degrees, the force of the forward and aft propeller repeat themselves. On the basis of Nyquist Sampling Theory, 396 data points can express the 198 periods in one revolution; for more accurate results, at least 5 data points are needed to reconstruct a period of fluctuation, which means that 990 data points are enough for this DCRP, and the 0.364-degree interval (*i.e.* 990 data points) is enough to resolve fluctuations at the lowest frequency. However, we find in Tab.6 that the time-step size of 1.5×Δt (corresponding to 1.5-degree interval) is enough for the numerical simulation accuracy. The reason is that the amplitudes of force fluctuations for this DCRP are expected to be less than 0.5% of the corresponding time-averages, according to the author's study (Cai *et al*, 2018). And it is very difficult to simulate the thrust and torque fluctuations at such a high frequency since their amplitudes are really small and easily contaminated by other numerical errors.

3.3 Hydrodynamic Performance Prediction of the DCRP

Fig.7 shows the time-averaged thrust and torque of the DCRP. It can be concluded that the thrust and torque are over-predicted for both forward and aft propeller, and the thrust is also over-predicted for the duct. The maximum error in predicted thrust is 7.37% for the CRP and the duct, while 5.87% in predicted torque. The maximum errors are 8.85% and 6.13% for the total thrust and torque respectively; the open-water efficiency is over-predicted with a maximum error of 4.04% in all J range.

4. Conclusions

A numerical prediction method for the hydrodynamic performance of DCRPs has been presented in the paper. A structured mesh based on unsteady RANS equations is applied, with the SST k-ω turbulence model employed. Boundary layer meshes are adopted on the CRP's blade surface and duct surface to improve the hydrodynamic performance prediction accuracy.

Numerical predictions are carried out for a DCRP utilized for a high-speed underwater vehicle. The mesh independence inspection and time-step size study are verified. In order to improve the prediction accuracy and to simulate or analyze the tip-clearance flow of the DCRP precisely, the structured mesh is advised to apply in the numerical simulation. An appropriate time-step size of 1.5×Δt is recommended for both the simulation accuracy and computation time.

Tab.6-Numerical simulation results with different time-step sizes

Time-step size	KT					KQ				
	Coarse	Medium	Fine	Fine-unstr	Model Test	Coarse	Medium	Fine	Fine-unstr	Model Test
3×Δt		0.5956	0.5852		0.5594		0.3412	0.3385		0.3246
2×Δt		0.5943	0.5841				0.3397	0.3369		
1.5×Δt	0.6470	0.5928	0.5830	0.6822		0.3508	0.3386	0.3361	0.3591	
Δt	0.6462	0.5923	0.5826	0.6820		0.3497	0.338	0.3358	0.3582	
0.5×Δt	0.6465	0.5925		0.6815		0.3503	0.3381		0.3579	

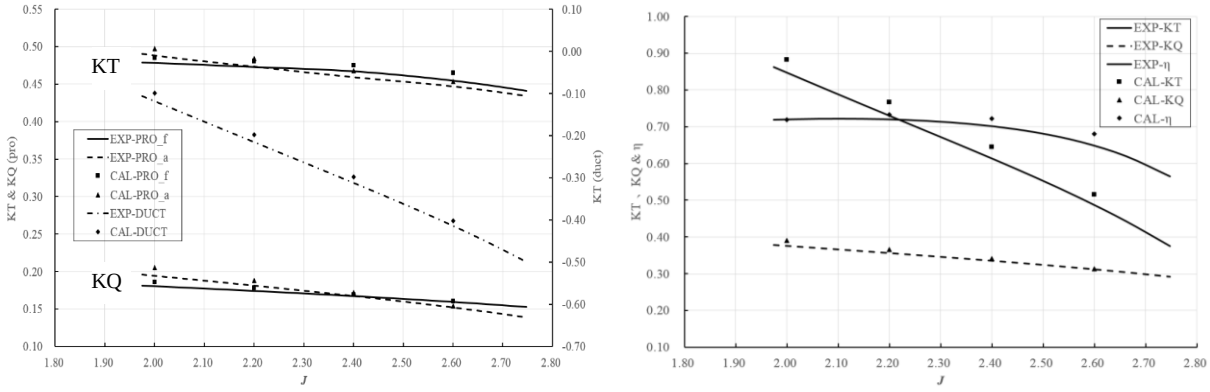

Fig.7-Comparison of the open-water performance of the DCRP obtained from unsteady simulations with experimental data

The predicted hydrodynamic performance is compared with available model test data. With verification, the numerical prediction method in this paper is capable of predicting the DCRP open-water performance with high accuracy.

Further researches are needed to simulate and analyze the hydrodynamic performance of DCRPs more precisely, including meshes generation strategy around the propeller tip, more suitable turbulence model, and different settings of numerical computation.

REFERENCES

Cai Hao-peng, Hao cheng-peng, Zhu xiao-meng and Zhang he (2018). 'Numerical prediction of unsteady hydrodynamic performance of contra-rotating propellers using RANS method'. Proceedings of the 13th International Conference on Hydornamics, Incheon, Korea.

Grassi, D., Brizzolara, S., Viviani, M., Savio, L. & Caviglia, S. (2013) 'Design and analysis of counter-rotating propellers comparison of numerical and experimental results'. Journal of Hydrodynamic, Ser. B, 22(5).

Gu, H. & Kinnas, S. A. (2003) 'Modeling of contra-rotating and ducted propellers via coupling of a vortex-lattice with a finite volume method'. Proceedings of Propellers/Shafting 2003 Symposium, Society of Naval Architects and Marine Engineers, Virginia, USA.

Henri Haimov, Jorge Vicario, & Javier Del Corral. (2011). 'RANSE code application for ducted and endplate propellers in open water'. Proceedings of the 2nd International Symposium on Marine Propulsors, Hamburg, Germany.

Hughes M. J, Kinnas S. A. (1991). 'An analysis method for a ducted propeller with pre-swirl stator blade'. Propellers/Shafting'91.

Ivanell, S. (2001). Hydrodynamic Simulation of a torpedo with Pump Jet Propulsion System. Master Thesis. Royal Institute of Technology, Stockholm, Sweden.

J. Baltazar, J.A.C. Falcão de Campos & J. Bosschers. (2011) 'Open-water thrust and torque predictions of a ducted propeller system with a panel method'. Proceedings of the 2nd International Symposium on Marine Propulsors, Hamburg, Germany.

Lin Lu, Guang Pan, & Prasanta K. Sahoo. (2016). 'CFD prediction and simulation of a pumpjet propulsor'. Int. J. Nav. Arch. Ocean. Eng. 8.

Liu X-L. (2009) 'A potential based panel method for prediction of steady and unsteady performances of contra-rotating propellers'. Proceedings of the 1st International Symposium on Marine Propulsors, Trondheim, Norway.

Menter, F. R. (1994). 'Two-equation eddy-viscosity turbulence models for engineering applications'. AIAA Journal, 32(8).

Motallebi-Nejad M, Bakhtiari M, & Ghassemi H, et al. (2017). 'Numerical analysis of ducted propeller and pumpjet propulsion system using periodic computational domain'. Journal of Marine Science & Technology, (3).

Rao Zhiqiang. (2012) Numerical Simulation of Hydrodynamical Performance of Pump Jet Propulsor. Master Thesis. Shanghai Jiao Tong University, Shanghai, china.

R. Bontempo, M. Cardone, & M. Manna. (2016). 'Performance analysis of ducted marine propellers.Part I – Decelerating duct'. Applied Ocean Research 58.

Sasaki, N., Kuroda, M., Fujisawa, J., Imoto, T. & Sato, M. (2009) 'On the model tests and design method of hybrid CRP podded propulsion system of a feeder container ship'. Proceedings of the 1st International Symposium on Marine Propulsors, Trondheim, Norway.

Su Y-r, Kinnas, S. A., & Jukola, H. (2017) 'Application of a BEM/RANS Interactive Method to Contra-Rotating Propellers'. Proceedings of the 5th International Symposium on Marine Propulsion, Espoo, Finland.

Suryanarayana, Ch, Satyanarayana, B., Ramji, K., Saiju, A. (2010a). 'Experimental evaluation of pumpjet propulsor for an axisymmetric body in wind tunnel'. Int. J. Nav. Arch. Ocean. Eng. 2.

Suryanarayana, Ch, Satyanarayana, B., Ramji, K., Saiju, A. (2010b). 'Performance evaluation of an underwater body and pumpjet by model testing in cavitation tunnel'. Int. J. Nav. Arch. Ocean. Eng 2.

Tsakonas, S., Jacobs, W. R. & Liao, P. (1983) 'Prediction of steady and unsteady loads and hydrodynamic forces on contra-rotating propellers'. Journal of Ship Research, 27(3).

Wang, Z. Z. & Xiong Y. (2013) 'Effect of time step size and turbulence model on the open water hydrodynamic performance prediction of contra-rotating propellers'. China Ocean Eng., 27(2).

Yang, C. J., Tamashima, M., Wang, G. Q. & Yamazaki, R. (1991) 'Prediction of the steady performance of contra-rotating propellers by lifting surface theory'. Transactions of the West-Japan Society of Naval Architects, 82.

Yang, C. J., Tamashima, M., Wang, G. Q. & Yamazaki, R. (1992) 'Prediction of the unsteady performance of contra-rotating propellers by lifting surface theory'. Transactions of the West-Japan Society of Naval Architects, 83.

Zhang, T., Yang, C. J. & Song, B. W. (2010) 'Investigations on the numerical simulation method for the open-water performance of contra-rotating propellers based on the MRF model'. Journal of Ship Mechanics, 14(8).

Zhang, T., Yang, C. J., Song, B. W. & Chen, Y. Y. (2011) 'CFD simulation of the unsteady performance of contra-rotating propellers'. Journal of Ship Mechanics, 15(6).